Magnetic field evolution of the zero-energy mode in Bi islands deposited on Fe(Te,Se)

Kailun Chen, Chuanhao Wen, Zhiyong Hou, Huan Yang,* and Hai-Hu Wen†
National Laboratory of Solid State Microstructures and Department of Physics, Collaborative Innovation Center of Advanced Microstructures, Nanjing University, Nanjing 210093, China

(Received 22 April 2024; revised 5 July 2024; accepted 26 July 2024; published 13 August 2024)

We investigate the magnetic-field dependence of the magnitude of zero-bias conductance peaks (ZBCPs) on some nanoscale bismuth islands grown on the $FeTe_{0.55}Se_{0.45}$ substrate. The ZBCPs exist only on some of the islands with a diameter of 4–8 nm, and are likely to be the Majorana zero modes. Remarkably, the evolution of ZBCPs on these islands exhibits anomalous behavior under varying magnetic fields. The intensity of ZBCPs is first enhanced at weak fields and then suppressed as the fields further increase. We attribute the nonmonotonic evolution of the ZBCPs to the magnetic-field-enhanced topological edge states on these Bi islands. Our findings provide valuable insights into the probable origin of the Majorana zero modes in the Bi-island platform and the magnetic-field response of topological edge states.

DOI: 10.1103/PhysRevB.110.054510

I. INTRODUCTION

Majorana zero modes (MZMs) attract intensive interest because of the potential applications in fault-tolerant topological quantum computing [1–3], and these modes can be realized in topological superconductors. One effective method for achieving topological superconductivity is to induce superconductivity in the topologically insulating layer through the proximity effect from the adjacent superconductor [4]. For example, zero-energy modes are observed in vortex cores of the heterostructures composed by the topological insulator Bi_2Te_3 and the conventional superconductor $NbSe_2$ [5,6] or the iron-based superconductor Fe(Te,Se) [7]. In addition, MZMs are also observed at the ends of vortex lines in superconductors with topologically nontrivial bands, such as some iron-based superconductors [8–13] or other materials [14,15].

On the surface of a topologically nontrivial superconductor, topological edge states appear at its boundary [1,16], such as the twin boundary [17] or the step edge [18]. In one-dimensional systems, topological edge states can exist in a semiconducting or spin-orbit-coupled nanowire, as well as in a ferromagnetic metal neighboring to a superconductor [19], where they appear as MZMs. Experimental observations of these modes are realized at the ends of one-dimensional semiconducting nanowires [20,21] and magnetic atomic chains [22] grown on the surface of an *s*-wave superconductor. As for two-dimensional heterostructures, MZMs [23] or Majorana edge modes [24,25] are observed on ferromagnetic islands grown on *s*-wave superconductors. In addition, a robust zero-energy mode is observed in a trilayer heterostructure $MnTe/Bi_2Te_3/Fe(Te,Se)$ [26].

Bismuth is a semimetal with strong spin-orbit coupling, and it is a good platform for investigating the topological superconductivity or the MZMs when it is adjacent to a superconductor. The Majorana edge states may exist at the boundary of the Bi layer with the former mentioned configuration. The experimental evidence has been demonstrated at the edges of Bi bilayers [27] and Bi films decorated with magnetic iron clusters [28] grown on the superconducting substrate. In our previous research, robust zero-energy modes were observed on specific Bi islands deposited on the iron-based superconductor Fe(Te,Se) [29]. The zero-energy modes are likely caused by the interference of two counterpropagating topological edge states at the boundary of Bi islands. This kind of edge state in a topologically nontrivial system is protected by time-reversal symmetry and is impervious to impurity scattering in the absence of magnetic fields. Therefore, after applying varying magnetic fields, the evolution of the edge states is also an interesting issue that has been scarcely reported in experiments.

In this paper, we examine the evolution of the ZBCP magnitude on some Bi islands grown on the $FeTe_{0.55}Se_{0.45}$ substrate when applying magnetic fields. Based on the statistics of all the measuring areas, the ZBCPs exist only on some of the islands with a diameter of 4–8 nm. The characteristics of the ZBCPs are also consistent with those of MZMs, indicating a topologically nontrivial origin of the ZBCPs. Notably, we observe an anomalous, yet general behavior of the ZBCPs relying on varying magnetic fields: The intensity of the ZBCPs on Bi islands is first enhanced at weak fields and subsequently decreases as the fields further increase. The strengthening of the ZBCPs at weak fields lower than 2 T may be attributed to the magnetic-field tuning of the Bessel function of the edge states to the inner part of the island or influenced by the superconducting current surrounding the vortex cores on the Fe(Te,Se) substrate.

II. EXPERIMENTAL METHODS

The single crystals of $FeTe_{0.55}Se_{0.45}$ were synthesized by the self-flux method [30]. The crystals were annealed at 400 °C for 20 h in an O_2 atmosphere to eliminate the

*Contact author: huanyang@nju.edu.cn
†Contact author: hhwen@nju.edu.cn

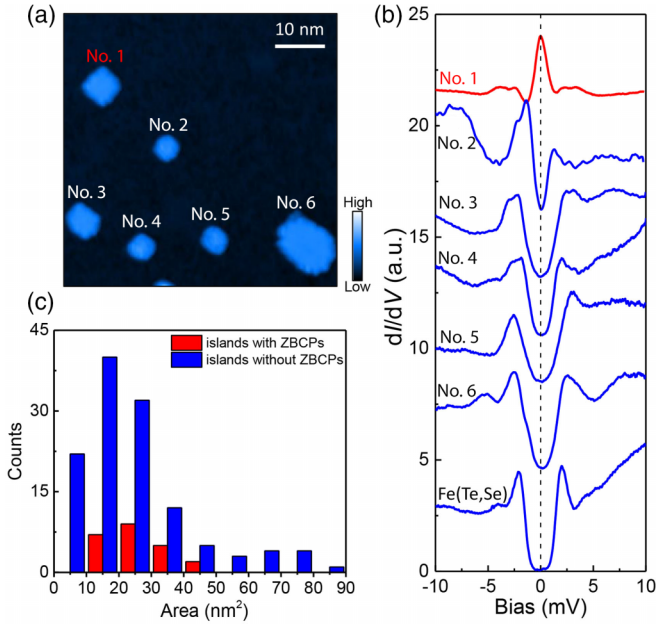

FIG. 1. (a) Topography of an area containing six Bi islands grown on the Fe(Te,Se) substrate (setpoint conditions: $V_{set} = 1$ V, $I_{set} = 20$ pA). (b) Typical tunneling spectra measured on the islands and the substrate nearby ($V_{set} = 10$ mV, $I_{set} = 200$ pA). Island No. 1 is the only one with ZBCP. (c) Statistics on the number of islands with and without ZBCPs versus the area for all islands we have measured.

interstitial Fe atoms and then quenched in the liquid nitrogen. The single crystal was cleaved in an ultrahigh vacuum with a pressure of about 1×10^{-10} Torr before the growth of the Bi islands. High-purity Bi (99.999%) powders were heated to 360 °C in the effusion cell (CreaTec) and then evaporated to the cleaved surface of Fe(Te,Se) at room temperature by molecular beam epitaxy method. The nanoscale bismuth islands can be grown on the Fe(Te,Se) substrate. Afterwards, the sample was transferred to the scanning tunneling microscopy/spectroscopy (STM/STS) head which was kept at a low temperature. The STM/STS measurements were carried out in a USM-1300 system (Unisoku Co. Ltd.) with an ultrahigh vacuum, low temperature, and high magnetic field. The tunneling spectra were measured by a lock-in technique with an amplitude of 0.2 mV and a frequency of 938 Hz. The tips in the measurements were made from tungsten using the electrochemical etching method. All measurements were taken at 0.4 K unless stated otherwise. The magnetic field was applied along the c axis of Fe(Te,Se) substrate or equivalently perpendicular to the Bi islands.

III. RESULTS

A. Bi islands with and without ZBCPs

Figure 1(a) shows a typical topography of the Bi islands grown on the Fe(Te,Se) substrate. The islands distribute randomly on the flat surface of the substrate with the dimensions of several nanometers. The shapes of these islands are also irregular, and there are even some wrinkles near the boundary indicating the lattice distortion there. The surface structure of most islands is distorted orthorhombic with lattice parameters of about 4.5–4.8 Å [29], which is consistent with the case of the top Bi atoms of a Bi(110) bilayer [31–33]. The heights of most islands are all about 7 Å, and this value is also similar to the thickness of the bilayer Bi(110) film [32,33]. Therefore, most Bi islands in the present work are likely to consist of Bi(110) bilayer films, but the lattice is distorted due to the mismatch of the Bi(110) film and the Fe(Te,Se) substrate. These features of the Bi islands are consistent with those in our previous work [29]. Since the Bi(111) islands are very rare, we focus on the Bi(110) bilayer island in the present paper.

Figure 1(b) shows typical tunneling spectra measured on the six islands in the field of view of Fig. 1(a). We also show the typical tunneling spectrum measured on the Fe(Te,Se) substrate in Fig. 1(b), and it shows a fully gapped feature. The superconducting gap of the Fe(Te,Se) substrate varies from 1.1 to 2.1 meV, determined by calculating the energy difference between coherence peaks [34]. Tunneling spectra measured on Bi islands Nos. 2–6 are similar to the ones measured on the Fe(Te,Se) substrate. However, the tunneling spectrum measured on island No. 1 is different, i.e., a ZBCP appears in the tunneling spectrum measured on this island. It should be noted that the ZBCP can be observed in the spectra measured on the whole island [29]. We have investigated 146 Bi bilayer islands, and only 23 of them hold ZBCPs. The probability of finding a Bi island with the ZBCPs is about 16%. We try to search for regular structural characteristics of the Bi bilayer islands with ZBCPs; however, it is difficult to find any special features. In Fig. 1(a), one can see that the edges of all the Bi islands are irregular with some structure of defects and protrusions [29]. In other words, the well-defined edges can hardly be observed on Bi islands grown on Fe(Te,Se). Meanwhile, there are also many defects on all the Bi(110) bilayer islands. We cannot get the relationship between the defect density and the existence of the ZBCPs, either. The existence of the irregular edges and dense defects is probably due to the large mismatch between the lattice structures of the Bi islands and the Fe(Te,Se) substrate. However, we do think that the appearance of ZBCPs is related to the edge and defect status of the Bi islands. We also note that there are some Bi islands with the height of two bilayers, but none of them hold the ZBCPs. The number statistics are also carried out in the region of Bi islands, and the result is shown in Fig. 1(c). One can see that the area of islands with ZBCPs mainly distributes from 10 to 50 nm^2, corresponding to a diameter of about 4–8 nm. When the areas of Bi islands exceed 50 nm^2, no ZBCPs have been observed in these islands.

Figure 2(a) shows the topography of nanoscale Bi island No. 7. The ZBCPs can be observed in the tunneling spectra measured on the island, just as in two spectra measured at the edge or the center of the island shown in Fig. 2(b). Besides, the energies of the coherence peaks of these two spectra are similar to those obtained from the spectra measured on the Fe(Te,Se) substrate, demonstrating the proximity-induced superconductivity on the Bi island. It should be noted that the ZBCP can be observed in the spectra taken all over the island, and one can obtain the conclusion from a set of tunneling spectra measured across the island as shown in Fig 2(c). Obvious in-gap peaks can be seen in all the spectra in this

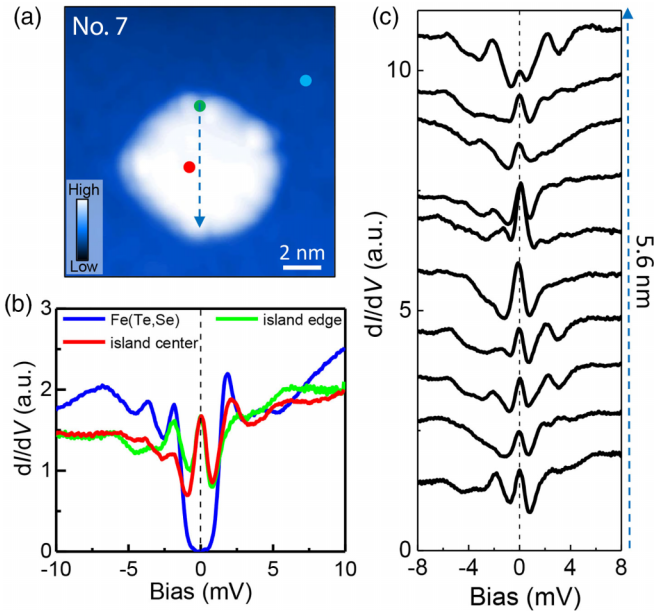

FIG. 2. (a) Topography of a Bi island (No. 7) ($V_{set} = 1$ V, $I_{set} = 20$ pA). (b) Typical tunneling spectra measured at marked positions shown in (a) ($V_{set} = 10$ mV, $I_{set} = 200$ pA). (c) Line profile of tunneling spectra taken along the dashed arrow in panel (a) ($V_{set} = 10$ mV, $I_{set} = 200$ pA).

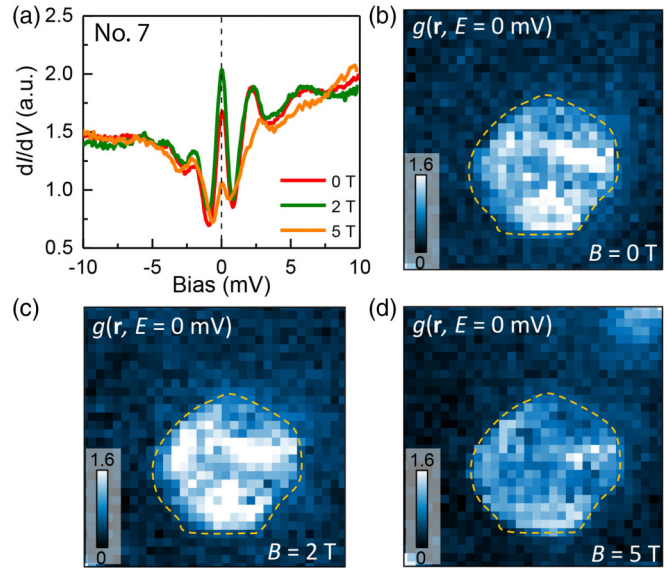

FIG. 3. (a) Tunneling spectra measured at different magnetic fields and at the location of the red dot in Fig. 2(a) ($V_{set} = 10$ mV, $I_{set} = 200$ pA). (b)–(d) Zero-energy dI/dV mappings recorded in the same region in Fig. 2(a), and they are measured at different fields ($V_{set} = 40$ mV, $I_{set} = 200$ pA). The edge of the island is marked out by dashed lines. The color bars are the same in these mappings.

panel, and the peak positions are fixed near zero energy. These observations are similar to those in our previous work [29].

B. Magnetic-field dependent evolution of ZBCPs on Bi islands

The ZBCPs on some Bi islands are weakened by an increase in temperature [29], which can be understood as the temperature suppression to the superconductivity in the Fe(Te,Se) substrate. Since the upper critical field of Fe(Te,Se) is extremely high [35], it is interesting to investigate the field-dependent evolution of the ZBCPs on the Bi islands. Figure 3(a) shows tunneling spectra measured at different fields of 0, 2, and 5 T at the center of Bi island No. 7. Surprisingly, the increment of the magnetic field does not suppress the ZBCP monotonically and, conversely, the peak magnitude increases at 2 T compared to that obtained at 0 T. At a higher field of 5 T, the magnitude of the ZBCP is significantly suppressed, but the ZBCP does not show any splitting or broadening features.

The differential conductance mapping is a useful method to get information on the spatial distribution of density of states (DOS) [36,37]. Figures 3(b)–3(d) show the recorded spatial distributions of zero-bias differential conductance of Bi island No. 7 in the same area but under different fields. These three mappings are presented in the same color scale, thus the brightness directly corresponds to the zero-energy DOS. The zero-bias differential conductance is almost zero on the Fe(Te,Se) substrate, reflecting the fully gapped feature. The value is finite on the whole island at 0 T, which corresponds to the robust zero mode on the island. Some weak ZBCP magnitude may be due to the surface-lattice distortion of the Bi islands. At the magnetic field of 2 T [Fig. 3(c)], the inner part of the island becomes notably brighter, suggesting an increment of the ZBCP magnitude. However, at 5 T [Fig. 3(d)], the zero-energy differential conductance becomes much weaker. These observations are consistent with the ZBCP evolution in the tunneling spectra at different fields shown in Fig. 3(a).

A control experiment is carried out on Bi island No. 8, and Fig. 4(a) shows the tunneling spectra measured at the same position but under different magnetic fields. The magnitude of the ZBCP increases when the magnetic field increases from 0 to 2 T, and then the value decreases as the field further increases. Similar experiments are also carried out on the other four islands Nos. 9–12, and the field-dependent zero-bias differential conductance is shown in Fig. 4(b). Here, it should be mentioned that these data are recorded in the Bi islands away from vortex cores in the Fe(Te,Se) layer; otherwise, the tunneling spectra behave very differently from the spectra measured at other neighbored fields. The curves in Fig. 4(b) share similar features with varying magnetic fields: the intensity of the ZBCP increases with increasing field and reaches its maximum at about 2 T and, afterward, the ZBCP magnitude decreases rapidly with the increase of the field. Therefore, the nonmonotonic field evolution of the ZBCP magnitude is a common property on these Bi islands grown on Fe(Te,Se).

IV. DISCUSSION

As presented above, we have investigated the magnetic-field dependence of the ZBCP magnitude on some Bi islands grown on the superconducting $FeTe_{0.55}Se_{0.45}$ substrate. On these specific islands with a size of 4–8 nm, the appearance of the zero-energy peak is the common feature of the spectra measured throughout the entire island. In the process of

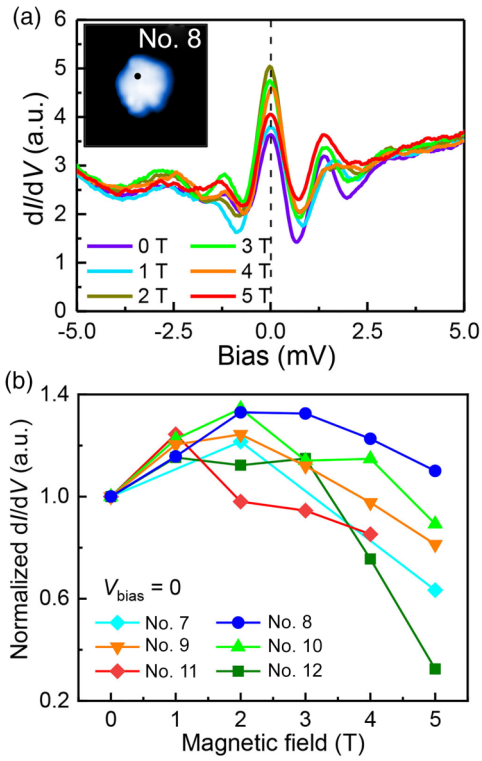

FIG. 4. (a) Tunneling spectra measured on another island No. 8 at different magnetic fields ($V_{set} = 10$ mV, $I_{set} = 200$ pA). The topography of the island is shown in the inset, and the spectra are measured at the marked position on the island. (b) Magnetic-field dependence of the ZBCP intensity on several islands with ZBCPs. The values of the zero-energy differential conductance at different fields are normalized by the value at zero field.

applying magnetic fields, the ZBCPs are fixed at zero energy and do not split. Additionally, the width of the ZBCPs does not broaden. These features exclude the trivial origin of the ZBCPs caused by Yu-Shiba-Rusinov states or the Andreev bound states [38] and are consistent with the characteristic of MZMs as reported previously [6,38–40]. Thus, the ZBCPs on the Bi islands probably have a topologically nontrivial origin. As discussed before [38], the ZBCPs may be due to the magnetic moment just below the particular Bi island. The magnetic moment can be induced by an interstitial iron atom, and it leads to the time-reversal symmetry breaking [19]. However, in the present paper, the ZBCP magnitude increases with the increase of magnetic field and reaches its maximum at about 2 T; afterwards, the magnitude decreases with increasing field. This is very different from the situation of excess iron impurities, and the ZBCP magnitude is almost stable or slightly decreased at a field as high as 8 T [39]. In addition, the effective range by the excess iron atom is very limited with a radius of about 1 nm [39], which is much smaller than the size of the Bi island. Therefore, the excess iron atom as the origin can be excluded, and the ZBCP is likely caused by the topological superconductivity induced on the Bi island with a strong spin-orbital coupling.

From our previous study [38], the zero-energy states observed on these Bi islands may be caused by two counterpropagating topological edge states [41] emerging at the edge of the islands. The edge state at about 100 meV was observed on very large bilayer Bi(110) islands grown on the HOPG substrate [31], and the bound state is clear because the bulk state and the substrate show the insulating behavior in the energy window. Bi is proved to be a second-order topological insulator [42], and some boundaries of Bi(110) facets can host such bound modes at about 100 meV due to a higher-order topology [43]. Here, from the tunneling spectra measured in Fe(Te,Se), there is a hump structure appearing at about 100 meV in the V-shaped background [7]. Due to such an electronic structure at a similar energy, it is difficult to determine whether the edge state exists on the Bi(110) island grown on Fe(Te,Se). However, due to the observation of the ZBCP, we argue that the edge state is likely to exist on the Bi(110) island.

The edge states usually behave as the spatial (r) oscillation of the Bessel function of $J_0^2(k_F r)$. Here, $J_0(x)$ is the zero-order Bessel function, and k_F is the Fermi wave vector. Since k_F is very small in Bi, the real-space period ($\sim \pi/k_F$) can be the scale of several nanometers [31]. The measured range of edge state from the island edge is about 2 nm [31] or more [43] in very large Bi(110) islands. The Bi islands are very small with a diameter of 4–8 nm in the present work; a pair of the edge states may form an interfered resonant state that behaves as the ZBCP. Based on this picture, the applied magnetic fields can tune the real-space period of the oscillation [44]. For a constant and small value of distance r, $J_0^2(k_F r)$ is positively correlated with k_F. To obtain the magnetic-field-dependent ZBCP amplitude, we adopt the model for the Majorana zero mode [44,45]. Since the island is very small and thin, there may be a tiny gap Λ opening near the Dirac point when considering the coupling of two branches of Dirac cones from the two edges of the island. A magnetic field of B equals an energy scale of $m \sim \mu_B B$ with μ_B the Bohr magneton, and a field of 2 T is equivalent to an energy of about 0.01 meV. Then the applied field affects the Fermi wave vector following the relationship of $k_F' = k_F\sqrt{1-(\frac{\Lambda-m}{\mu})^2}$, with μ the chemical potential of the surface state. With the increase of B or m, k_F' increases and reaches its maximum when m is close to $\Lambda \sim 0.01$ meV; afterward, k_F' decreases with increase of B. This makes a nonmonotonic field dependence of k_F' and further the ZBCP amplitude. It should be noted that this is a very rough estimation of the field-dependent ZBCP amplitude especially when we do not know the exact origin of the ZBCP, but the rough estimation may help us to understand the nonmonotonic field-dependent behavior of ZBCP amplitude. Meanwhile, the edges of all the Bi islands are irregular with some structure of defects and protrusions as mentioned above. Considering Bi islands may be second-order topological insulators [42], these islands would naturally possess discontinuous topological edge states with several ends [27,43]. However, the edges are not well-defined on the Bi islands here, and the edge states may be blocked by many boundary ends. It is possible that these ends of topological edge states with proximity-induced superconductivity play a crucial role in the presence of ZBCPs. However, the nonmonotonic field evolution of the ZBCPs requires further investigation based on this picture.

Another possibility of the nonmonotonic evolution of the ZBCP magnitude is from the vortex core in the Fe(Te,Se)

substrate. Although our tunneling spectra are recorded when the Bi island is away from the vortex core in Fe(Te,Se), there are also some vortex cores nearby. One of them is shown in the upper right corner of Fig. 3(d). The superconducting current surrounding the vortex cores may pass through the Fe(Te,Se) underneath, which probably enhances the edge states on the Bi island and induces an increment of the ZBCP magnitude. At higher magnetic fields, the ZBCP magnitude decreases because of the suppression of topological edge states and/or the suppression of proximity-induced superconductivity under high magnetic fields. However, further theoretical consideration is required to understand the nonmonotonic relationship between the ZBCP magnitude and the magnetic field quantitatively, as well as the reason why ZBCPs only appear on specific Bi islands.

V. CONCLUSION

In summary, we have observed the MZMs on certain Bi islands with a diameter of 4–8 nm deposited on the $FeTe_{0.55}Se_{0.45}$ substrate. Further experiments on these islands under varying magnetic fields reveal an unusual behavior of the ZBCP magnitude. Specifically, the intensity is initially enhanced at weak fields, but then becomes suppressed as the field strength increases. This nonmonotonic evolution of the ZBCP magnitude is different from the monotonically decreased magnitude with the increasing field for the ZBCP observed in the iron impurity [39,45], the magnetic monolayer film in the trilayer heterostructure [26,44], or the vortex core in Fe(Te,Se) [38]. The anomalous evolution of ZBCP here is probably caused by the magnetic-field tuning of the Bessel function of the edge states or influenced by the superconducting current surrounding the vortex cores on the Fe(Te,Se) substrate. Our findings will be helpful in understanding the mechanism of the topological bismuth systems and shed light on the topological property of Majorana zero modes under magnetic fields.

ACKNOWLEDGMENTS

We appreciate very useful discussions with N. Hao. The work was supported by the National Natural Science Foundation of China (Grants No. 12061131001 and No. 11927809) and the National Key R&D Program of China (Grant No. 2022YFA1403201).

[1] X. L. Qi and S. C. Zhang, Topological insulators and superconductors, Rev. Mod. Phys. **83**, 1057 (2011).
[2] M. Sato and Y. Ando, Topological superconductors: A review, Rep. Prog. Phys. **80**, 076501 (2017).
[3] C. Nayak, S. H. Simon, A. Stern, M. Freedman, and S. Das Sarma, Non-Abelian anyons and topological quantum computation, Rev. Mod. Phys. **80**, 1083 (2008).
[4] L. Fu and C. L. Kane, Superconducting proximity effect and Majorana fermions at the surface of a topological insulator, Phys. Rev. Lett. **100**, 096407 (2008).
[5] H.-H. Sun and J.-F. Jia, Detection of Majorana zero mode in the vortex, npj Quantum Mater. **2**, 34 (2017).
[6] J.-P. Xu, M.-X. Wang, Z. L. Liu, J.-F. Ge, X. Yang, C. Liu, Z. A. Xu, D. Guan, C. L. Gao, D. Qian, Y. Liu, Q.-H. Wang, F.-C. Zhang, Q.-K. Xue, and J.-F. Jia, Experimental detection of a Majorana mode in the core of a magnetic vortex inside a topological insulator-superconductor heterostructure $Bi_2Te_3/NbSe_2$, Phys. Rev. Lett. **114**, 017001 (2015).
[7] M. Chen, X. Chen, H. Yang, Z. Du, and H.-H. Wen, Superconductivity with twofold symmetry in $Bi_2Te_3/FeTe_{0.55}Se_{0.45}$ heterostructures, Sci. Adv. **4**, eaat1084 (2018).
[8] D. F. Wang, L. Y. Kong, P. Fan, H. Chen, S. Y. Zhu, W. Y. Liu, L. Cao, Y. J. Sun, S. X. Du, J. Schneeloch, R. D. Zhong, G. D. Gu, L. Fu, H. Ding, and H.-J. Gao, Evidence for Majorana bound states in an iron-based superconductor, Science **362**, 333 (2018).
[9] T. Machida, Y. Sun, S. Pyon, S. Takeda, Y. Kohsaka, T. Hanaguri, T. Sasagawa, and T. Tamegai, Zero-energy vortex bound state in the superconducting topological surface state of Fe(Se, Te), Nat. Mater. **18**, 811 (2019).
[10] N. Hao and J. Hu, Topological quantum states of matter in iron-based superconductors: From concept to material realization, Natl. Sci. Rev. **6**, 213 (2019).
[11] Q. Liu, C. Chen, T. Zhang, R. Peng, Y.-J. Yan, C.-H.-P. Wen, X. Lou, Y.-L. Huang, J.-P. Tian, X.-L. Dong, G.-W. Wang, W.-C. Bao, Q.-H. Wang, Z.-P. Yin, Z.-X. Zhao, and D.-L. Feng, Robust and clean Majorana zero mode in the vortex core of high-temperature superconductor $(Li_{0.84}Fe_{0.16})$OHFeSe, Phys. Rev. X **8**, 041056 (2018).
[12] W. Liu, L. Cao, S. Zhu, L. Kong, G. Wang, M. Papaj, P. Zhang, Y.-B. Liu, H. Chen, G. Li, F. Yang, T. Kondo, S. Du, G.-H. Cao, S. Shin, L. Fu, Z. Yin, H.-J. Gao, and H. Ding, A new Majorana platform in an Fe-As bilayer superconductor, Nat. Commun. **11**, 5688 (2020).
[13] M. Li, G. Li, L. Cao, X. Zhou, X. Wang, C. Jin, C.-K. Chiu, S. J. Pennycook, Z. Wang, and H.-J. Gao, Ordered and tunable Majorana-zero-mode lattice in naturally strained LiFeAs, Nature (London) **606**, 890 (2022).
[14] Y. Yuan, J. Pan, X. Wang, Y. Fang, C. Song, L. Wang, K. He, X. Ma, H. Zhang, F. Huang, W. Li, and Q.-K. Xue, Evidence of anisotropic Majorana bound states in 2M-WS_2, Nat. Phys. **15**, 1046 (2019).
[15] Z. Liang, X. Hou, F. Zhang, W. Ma, P. Wu, Z. Zhang, F. Yu, J.-J. Ying, K. Jiang, L. Shan, Z. Wang, and X.-H. Chen, Three-dimensional charge density wave and surface-dependent vortex-core states in a kagome superconductor CsV_3Sb_5, Phys. Rev. X **11**, 031026 (2021).
[16] M. Z. Hasan and C. L. Kane, Colloquium: Topological insulators, Rev. Mod. Phys. **82**, 3045 (2010).
[17] Z. Wang, J. O. Rodriguez, L. Jiao, S. Howard, M. Graham, G. D. Gu, T. L. Hughes, D. K. Morr, and V. Madhavan, Evidence for dispersing 1D Majorana channels in an iron-based superconductor, Science **367**, 104 (2020).
[18] L. Jiao, S. Howard, S. Ran, Z. Wang, J. O. Rodriguez, M. Sigrist, Z. Wang, N. P. Butch, and V. Madhavan, Chiral

superconductivity in heavy-fermion metal UTe_2, Nature (London) **579**, 523 (2020).

[19] J. Alicea, New directions in the pursuit of Majorana fermions in solid state systems, Rep. Prog. Phys. **75**, 076501 (2012).

[20] V. Mourik, K. Zuo, S. M. Frolov, S. R. Plissard, E. Bakkers, and L. P. Kouwenhoven, Signatures of Majorana fermions in hybrid superconductor-semiconductor nanowire devices, Science **336**, 1003 (2012).

[21] M. T. Deng, S. Vaitiekenas, E. B. Hansen, J. Danon, M. Leijnse, K. Flensberg, J. Nygård, P. Krogstrup, and C. M. Marcus, Majorana bound state in a coupled quantum-dot hybrid-nanowire system, Science **354**, 1557 (2016).

[22] S. Nadj-Perge, I. K. Drozdov, J. Li, H. Chen, S. Jeon, J. Seo, A. H. MacDonald, B. A. Bernevig, and A. Yazdani, Observation of Majorana fermions in ferromagnetic atomic chains on a superconductor, Science **346**, 602 (2014).

[23] S. Kezilebieke, M. N. Huda, V. Vaňo, M. Aapro, S. C. Ganguli, O. J. Silveira, S. Głodzik, A. S. Foster, T. Ojanen, and P. Liljeroth, Topological superconductivity in a van der Waals heterostructure, Nature (London) **588**, 424 (2020).

[24] A. Palacio-Morales, E. Mascot, S. Cocklin, H. Kim, S. Rache, D. K. Morr, and R. Wiesendanger, Atomic-scale interface engineering of Majorana edge modes in a 2D magnet-superconductor hybrid system, Sci. Adv. **5**, eaav6600 (2019).

[25] G. C. Ménard, S. Guissart, C. Brun, R. T. Leriche, M. Trif, F. Debontridder, D. Demaille, D. Roditchev, P. Simon, and T. Cren, Two-dimensional topological superconductivity in Pb/Co/Si(111), Nat. Commun. **8**, 2040 (2017).

[26] S. Ding, C. Chen, Z. Cao, D. Wang, Y. Pan, R. Tao, D. Zhao, Y. Hu, T. Jiang, Y. Yan, Z. Shi, X. Wan, D. Feng, and T. Zhang, Observation of robust zero-energy state and enhanced superconducting gap in a trilayer heterostructure of $MnTe/Bi_2Te_3/Fe(Te, Se)$, Sci. Adv. **8**, eabq4578 (2022).

[27] I. K. Drozdov, A. Alexandradinata, S. Jeon, S. Nadj-Perge, H. Ji, R. J. Cava, B. A. Bernevig, and A. Yazdani, One-dimensional topological edge states of bismuth bilayers, Nat. Phys. **10**, 664 (2014).

[28] B. Jäck, Y. Xie, J. Li, S. Jeon, B. A. Bernevig, and A. Yazdani, Observation of a Majorana zero mode in a topologically protected edge channel, Science **364**, 1255 (2019).

[29] X. Chen, M. Chen, W. Duan, H. Yang, and H.-H. Wen, Robust zero energy modes on superconducting bismuth islands deposited on Fe(Te, Se), Nano Lett. **20**, 2965 (2020).

[30] Y. Liu and C. T. Lin, A comparative study of $Fe_{1+\delta}Te_{1-x}Se_x$ single crystals grown by Bridgman and self-flux techniques, J. Supercond. Novel Magn. **24**, 183 (2011).

[31] Y. Lu, W. Xu, M. Zheng, G. Yao, L. Shen, M. Yang, Z. Luo, F. Pan, K. Wu, T. Das, J. Jiang, J. Martin, Y. P. Feng, H. Lin, and X.-s. Wang, Topological properties determined by atomic buckling in self-assembled ultrathin Bi(110), Nano Lett. **15**, 80 (2015).

[32] T. Nagao, J. T. Sadowski, M. Saito, S. Yaginuma, Y. Fujikawa, T. Kogure, T. Ohno, Y. Hasegawa, S. Hasegawa, and T. Sakurai, Nanofilm allotrope and phase tansformation of ultrathin Bi film on Si(111)-7×7, Phys. Rev. Lett. **93**, 105501 (2004).

[33] P. Hofmann, The surfaces of bismuth: Structural and electronic properties, Prog. Surf. Sci. **81**, 191 (2006).

[34] M. Chen, X. Chen, H. Yang, Z. Du, X. Zhu, E. Wang, and H.-H. Wen, Discrete energy levels of Caroli-de Gennes-Matricon states in quantum limit in $FeTe_{0.55}Se_{0.45}$, Nat. Commun. **9**, 970 (2018).

[35] H. Lei, R. Hu, E. S. Choi, J. B. Warren, and C. Petrovic, Pauli-limited upper critical field of $Fe_{1+y}Te_{1-x}Se_x$, Phys. Rev. B **81**, 094518 (2010).

[36] Ø. Fischer, M. Kugler, I. Maggio-Aprile, C. Berthod, and C. Renner, Scanning tunneling spectroscopy of high-temperature superconductors, Rev. Mod. Phys. **79**, 353 (2007).

[37] J. E. Hoffman, Spectroscopic scanning tunneling microscopy insights into Fe-based superconductors, Rep. Prog. Phys. **74**, 124513 (2011).

[38] X. Chen, M. Chen, W. Duan, X. Zhu, H. Yang, and H.-H. Wen, Observation and characterization of the zero energy conductance peak in the vortex core state of $FeTe_{0.55}Se_{0.45}$, arXiv:1909.01686.

[39] J. X. Yin, Z. Wu, J. H. Wang, Z. Y. Ye, J. Gong, X. Y. Hou, L. Shan, A. Li, X. J. Liang, X. X. Wu, J. Li, C. S. Ting, Z. Q. Wang, J. P. Hu, P. H. Hor, H. Ding, and S. H. Pan, Observation of a robust zero-energy bound state in iron-based superconductor Fe(Te, Se), Nat. Phys. **11**, 543 (2015).

[40] P. Fan, F. Yang, G. Qian, H. Chen, Y. Y. Zhang, G. Li, Z. Huang, Y. Xing, L. Kong, W. Liu, K. Jiang, C. Shen, S. Du, J. Schneeloch, R. Zhong, G. Gu, Z. Wang, H. Ding, and H. J. Gao, Observation of magnetic adatom-induced Majorana vortex and its hybridization with field-induced Majorana vortex in an iron-based superconductor, Nat. Commun. **12**, 1348 (2021).

[41] A. P. Schnyder, S. Ryu, A. Furusaki, and A. W. W. Ludwig, Classification of topological insulators and superconductors in three spatial dimensions, Phys. Rev. B **78**, 195125 (2008).

[42] F. Schindler, Z. Wang, M. G. Vergniory, A. M. Cook, A. Murani, S. Sengupta, A. Yu. Kasumov, R. Deblock, S. Jeon, I. Drozdov, H. Bouchiat, S. Guéron, A. Yazdani, B. A. Bernevig, and T. Neupert, Higher-order topology in bismuth, Nat. Phys. **14**, 918 (2018).

[43] L. Aggarwal, P. Zhu, T. L. Hughes, and V. Madhavan, Evidence for higher order topology in Bi and $Bi_{0.92}Sb_{0.08}$, Nat. Commun. **12**, 4420 (2021).

[44] R. Song and N. Hao, Stealth Majorana zero mode in a trilayer heterostructure $MnTe/Bi_2Te_3/Fe(Te, Se)$, Phys. Rev. B **108**, L100509 (2023).

[45] R. Song, P. Zhang, X.-T. He, and N. Hao, Ferromagnetic impurity induced Majorana zero mode in iron-based superconductors, Phys. Rev. B **106**, L180504 (2022).